Sliding-Mode Control With Multipower Approaching Law for DC-Link Voltage of Z-Source Photovoltaic Inverters

YAN CHEN[1], RUI TAN [1], YONG ZHENG[2], AND ZHIYANG ZHOU[1]

[1]School of Electrical and Electronic Engineering, Chongqing University of Technology, Chongqing 400054, China
[2]Engineering Research Center of Mechanical Testing Technology and Equipment, Ministry of Education, Chongqing University of Technology, Chongqing 400054, China

Corresponding author: Yong Zheng (sdzzzy@cqut.edu.cn)

ABSTRACT Z-source photovoltaic inverters feature a unique topology and a special modulation strategy that enables a traditional two-stage system function through a single-stage structure. Therefore, Z-source inverters are expected to gain an extensive application when inputs change significantly. Given the objective of achieving DC-link voltage control based on small-signal model analyses, this study proposes a sliding-mode control method with a multipower approaching law (MPAL) for the DC-link control of inverters. This novel approach can solve the slow convergence rate and serious buffeting of the traditional sliding-mode control. The proposed approach makes the system state reach the sliding surface rapidly. The inherent buffeting of the sliding-mode control is simultaneously weakened and even eliminated in a few cases. The simulation and experimental analyses prove that the proposed sliding-mode control with an MPAL features significant advantages unlike the traditional sliding-mode control and provides a certain practical value.

INDEX TERMS Sliding-mode control, Z-source PV inverter, multipower approaching law, DC-link voltage control.

I. INTRODUCTION

As a result of the intermittent characteristics of solar energy, photovoltaic (PV) cells are influenced by ambient temperature and illumination intensity, and the output voltage fluctuates in a wide range. Therefore, traditional inverter technologies face serious challenges. The traditional two-stage inverter system has low efficiency, and the dead time for the shoot-through state limits the inverter capacity; these problems were addressed with a Z-source inverter proposed in 2003 [1]. A pair of inductors and capacitors were added to traditional inverters to form a Z-source network. Unlike traditional inverters, Z-source inverters offer the following advantages [2]: (1) Z-source inverters can boost voltage via the control of the shoot-through duty cycle of the Z-source network; (2) Z-source inverters have high reliability; (3) Z-source inverters are a single-stage system with a simple structure and high efficiency. These advantages

make Z-source inverters an extensively used technology in many fields of application, including PV generation systems with varying input voltages.

Scholars have mainly focused on the following aspects to broaden the application scope of Z-source inverters: (1) Improved topology: In [3]–[5], a few Z-source inverters with improved boost capability were proposed. In [6], a quasi-Z-source inverter was proposed to reduce the voltage stress of devices. In [7], [8], an isolated quasi-Z-source inverter was proposed; and (2) Optimized modulation and control strategies: A proportional-integral (PI) control strategy for stabilizing the voltage of Z-source capacitors was proposed in [9], A voltage constant control strategy that involved the control of capacitor voltage was proposed in [10]. This strategy was realized by controlling the Z-source inductor current in [11] to stabilize the output voltage of the Z-source network. A modulation strategy with a third harmonic injection reduced the voltage stress of a power device and the current ripple of the Z-source network inductor [12].

The associate editor coordinating the review of this manuscript and approving it for publication was Nishant Unnikrishnan.

Although existing research has improved the performance of Z-source topologies and expanded their application scope, a stable DC-link voltage ensures a stable Z-source inverter output. However, the DC link of a Z-source inverter is a pulsating square wave voltage that cannot be directly measured. Thus, a stable DC-link voltage is generally realized by indirectly controlling the Z-source network capacitor voltage. Such indirect control is disadvantageous because the DC-link voltage cannot be controlled directly. Moreover, Z-source converters are nonlinear systems; thus, the traditional PI single-loop control, double-loop control, and quasi-proportional-resonant control methods cannot reach static and dynamic characteristics. Sliding-mode control is an effective control strategy to solve the nonlinear problem. A sliding-mode control strategy for Z-source inverters was proposed to stabilize the DC-link voltage in [13], [14]. In [15], sliding-mode control was applied to a single-phase Z-source PV inverter system, thereby eliminating the influence of the non-minimum phase system while reducing the overshoot and oscillation of the Z-source capacitor voltage to ensure a high-quality current without distortion. However, the traditional sliding mode is prone to chattering [16], [17], which has been the focus of many studies [18], [19]. Approaching speed can be accelerated by controlling the approach law, and buffeting can be effectively reduced through an exponential approximation law [20]. In [21], exponential convergence and single-power approaching law were proposed to solve the problem of traditional power convergence rate. The double-power sliding-mode approximation proposed in [22] could make the system state variable converge rapidly and improve the approaching law. However, this paper did not present an analysis of the approximation law. An improved double-power convergence law was proposed in [23] to accelerate the approaching law. The proposed law could improve the convergence rate when the initial state $|s_0|$ is above 1. In [24], a multipower approximation law was proposed. Three different approach rates were employed in the system-approaching process via phased adjustments. An improved approaching law was achieved without buffeting.

Existing research indicates that the multipower approaching law (MPAL) for sliding-mode control can hasten dynamic response and improve the characteristics of the capacitor voltage, system output voltage, current, and system robustness. Unlike the traditional control methods for Z-source DC-link voltage, MPAL can effectively stabilize the DC-link peak voltage. Moreover, the method is applicable to the Z-source family topology.

II. PRINCIPLE OF Z-SOURCE PHOTOVOLTAIC INVERTERS

A Z-source PV inverter is shown in Fig. 1, where R and r are the equivalent resistances of the capacitance and inductance series, respectively.

Z-source PV inverters can be controlled in a straight-through state. Thus, such inverters have two operating modes, namely, shoot-through and non-shoot-through modes.
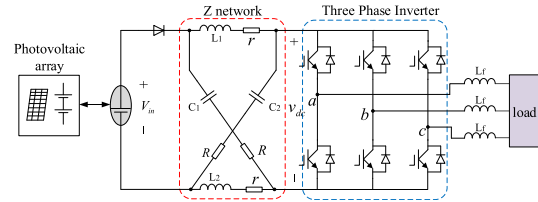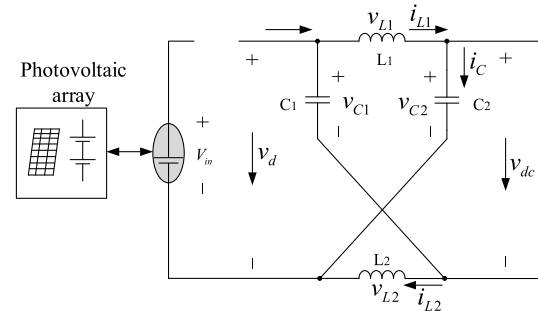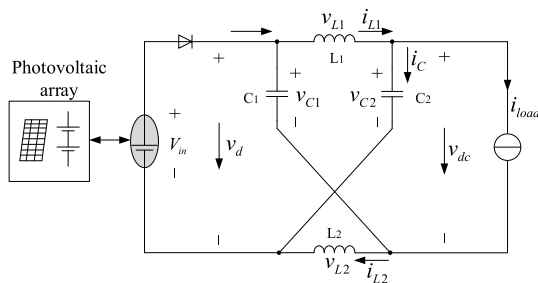

FIGURE 1. System structure of a Z-source inverter.

(a) Equivalent circuit of the shoot-through mode

(b) Equivalent circuit of the non-shoot-through mode

FIGURE 2. Equivalent circuit of the Z-source PV inverter.

Figure 2 shows an equivalent model ignoring R and r: V_{in} is the DC side of the input voltage generated by the PV array, v_L is the inductor voltage, v_C is the capacitor voltage, v_{dc} is the DC-side voltage, i_{load} is the load current, and i_L is the inductor current.

The Z-source network is symmetrical in the steady state. In the analysis, the following assumptions are used for the Z-source network: $C_1 = C_2 = C$, and $L_1 = L_2 = L$. The following equation is obtained from Fig. 2 (a):

$$v_L = V_C; v_d = v_L + V_C = 2 \times V_C; v_{dc} = 0 \qquad (1)$$

$$i_C = -I_L \qquad (2)$$

where V_C and I_L are the average values of the capacitor voltage and the inductance current, respectively. The following equation is obtained based on Fig. 2 (b):

$$v_L = V_{in} - V_C; v_{dc} = V_C - v_L = 2 \times V_C - V_{in} \qquad (3)$$

$$i_C = I_L - I_{load} \qquad (4)$$

where I_{load} is the Z-source network that outputs the current average to the inverter in the non-shoot-through mode.

The shoot-through and non-shoot-through duty ratios are D and $1 - D$, respectively. The average voltage in the steady state is 0 based on the volt-second balance principle, i.e.,

$$\bar{v}_L = V_C \times D + (V_{in} - V_C) \times (1 - D) = 0 \quad (5)$$

$$V_C = \frac{1 - D}{1 - 2D} \times V_{in} \quad (6)$$

The integral in a switching cycle for the capacitor current is 0. In the steady state, the integral can be written as follows:

$$I_L = \frac{1 - D}{1 - 2D} \times I_{load} \quad (7)$$

The non-shoot-through state expression is as follows: $V_{dc} = 2 \times V_C - V_{in} = \frac{1}{1-2D} \times V_{in}$. Therefore, in the case of a certain input voltage, the inverter output voltage can be changed by setting a different duty cycle D (i.e., $D < 0.5$).

III. DC-LINK VOLTAGE CONTROL

In analyzing the dynamic performance of the Z-source network, a small-signal model is established with the state space averaging method. Thereafter, the Laplace transform of the model is obtained. The transfer function of the shoot-through duty ratio D to the capacitor voltage is as follows:

$$\frac{\hat{V}_c(s)}{\hat{D}_c(s)} = \frac{(1 - 2D)(2V_C - V_{in} - R_L I_{load}) + (I_{load} - 2L)(Ls + R + r)}{S^2 \cdot LC + (R + r) \cdot C \cdot s + (1 - 2D)^2} \quad (8)$$

where R_L is the equivalent load resistance. The relationship between the capacitor voltage and the DC link voltage is as follows: $\frac{V_{dc}}{V_C} = \frac{1}{1-D}$. The small-signal transfer function of the duty ratio D to the DC-link voltage is as follows: The equations are as follows:

$$a = -V_{dc} \cdot LC$$
$$b = (I_{load} - 2I_L) \cdot L - V_{dc} \cdot (R + r) \cdot C$$
$$c = (1 - 2D)(2V_C - V_{in} - R_L \cdot I_{load})$$
$$+ (I_{load} - 2I_L) \cdot (R + r) - V_{dc} \cdot (R + r) - V_{dc} \cdot (1 - 2D)^2 \quad (9)$$

The analysis of the preceding transfer function reveals the existence of the right-half-plane zero in the system, thereby showing a non-minimum phase. Under such a condition, the output of the Z-source capacitor voltage and the DC-link voltage is overly controlled. The effect of the non-minimum phase on the system becomes increasingly evident with oscillation that occurs when the input is abruptly disturbed, particularly under large perturbation.

The stability of the DC-link voltage is determined by the zero-pole distribution of the system transfer function. Thus, V_{dc} should be constant when the output is stable. Given that V_{dc} is a pulsating square wave voltage, which is difficult to measure, it can be derived from a $V_{dc} = 2 \times V_C - V_{in}$. Accordingly, V_{dc} can be obtained indirectly by measuring the capacitance voltage. When V_{dc} is ensured to be constant, the reference value of the capacitor voltage can be derived as $V_C^* = \frac{V_{dc} + V_{in}}{2}$.
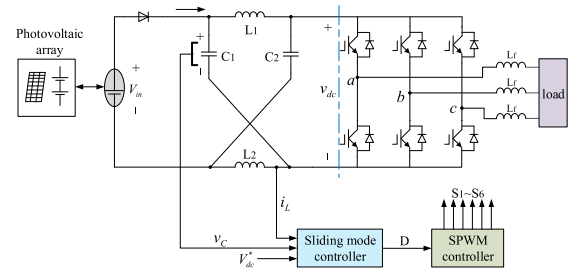
(a) Schematic diagram of the sliding mode control
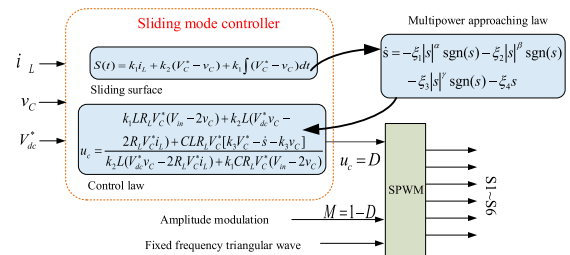
(b) Inverter switching controller

FIGURE 3. Sliding mode control system of the Z-source photovoltaic inverter.

The difference between V_C^* and the actual capacitor voltage is considered a variable to construct the sliding-mode controller, thereby ensuring a constant DC-link voltage V_{dc}.

IV. SLIDING-MODE CONTROLLER DESIGN

The sliding-mode control system of the DC-link voltage is shown in Fig. 3. A simple modulation method is used in this study. Under this method, two lines (i.e., V_p and V_n) are added to the sinusoidal pulse-width modulation. These lines are symmetrical based on the horizontal axis. V_p is equal to the amplitude of the modulation wave M. Thus, $M = 1 - D$, $V_P = 1 - D$, and $V_n = D - 1$. The control block diagram of the sliding mode controller is shown in Figure 3(b). It includes the design of the sliding surface and the approach law.

A. SLIDING SURFACE DESIGN

The following state variables of the Z-source network are selected:

$$\begin{bmatrix} \dot{x}_1 \\ \dot{x}_2 \\ \dot{x}_3 \end{bmatrix} = \begin{bmatrix} \frac{2v_C - V_{in}}{L} \\ \frac{2i_L}{C} - \frac{V_{dc}^* v_C}{R_L C V_C^*} \\ 0 \end{bmatrix} u + \begin{bmatrix} \frac{-v_C + V_{in}}{L} \\ \frac{V_{dc}^* v_C}{R_L C V_C^*} - \frac{i_L}{C} \\ V_C^* - v_C \end{bmatrix} \quad (10)$$

where u is the control variable, $x_1 = i_L$, $x_2 = V_C^* - v_C$, and $x_3 = \int (V_C^* - v_C)dt$.

The sliding surface function is selected as follows:

$$s = k_1 \times x_1 + k_2 \times x_2 + k_3 \times x_3 \quad (11)$$

where k_1, k_2, and k_3 are the sliding-mode coefficients that satisfy the Hurwitz condition. Therefore,

$$\dot{s} = k_1 \times \dot{x}_1 + k_2 \times \dot{x}_2 + k_3 \times \dot{x}_3 \quad (12)$$

The design of parameters k_1, k_2, and k_3 must ensure that the system can reach the sliding surface at any initial state.

Lyapunov stability theory states that a sliding-mode control law is designed to satisfy approximation conditions [25]. The Lyapunov function is selected as follows:

$$v = \frac{1}{2}s^2 \tag{13}$$

We obtain $\dot{v} = s \times \dot{s}$ based on the derivation of the preceding function. Lyapunov stability theory also indicates that if the system from any initial state in a limited period reaches the sliding surface, then $\dot{v} \leq 0$ is constant. However, in practical applications, the equal sign is often removed, i.e., $s \times \dot{s} < 0$. The working state of the Z-source inverter features an onÍCoff switch among different modes. Thus, the following switch function is defined:

$$u = \begin{cases} 0 & non-shoot-through\ mode, \quad when\ s > 0 \\ 1 & shoot-through\ mode, \quad when\ s < 0 \end{cases} \tag{14}$$

(1) When $s < 0$, $u = 1$,

$$\dot{s} = k_1 \times \frac{v_C}{L} + k_2 \times \frac{i_L}{C} + k_3 \times (V_C^* - v_C) \tag{15}$$

In the neighborhood of sliding surface, $v_C \approx V_C^*$, and $i_L \approx I_L^*$, thus, $V_C^* - v_C$ is very small. Given through duty ratio $D < 0.5$, combining Formulas (6) and (7), we can obtain $V_C > 0$ and $I_L^* > 0$. In the neighborhood of sliding surface, $v_C > 0$ and $i_L > 0$. Therefore, when $k_1, k_2 > 0$, in the neighborhood of sliding surface, $\dot{s} > 0$ must exist.

(2) When $s > 0$, $u = 0$,

$$\dot{s} = k_1 \times \frac{V_{in} - v_C}{L} + k_2 \times (\frac{V_{dc}^* v_C}{R_L C V_C^*} - \frac{i_L}{C}) + k_3 \times (V_C^* - v_C) \tag{16}$$

Similarly, in the neighborhood of sliding surface, the value of $V_C^* - v_C$ is very small, and

$$\frac{V_{dc}^* v_C}{R_L V_C^*} - i_L = I_{load} - i_L = -i_C \approx 0$$

. $V_{in} - v_C < 0$ can be obtained according to Formula (6). Thus, when $K_1 > 0$, in the neighborhood of sliding surface, $\dot{s} < 0$ must exist. Combining (1) and (2), we can determine that when $k_1, k_2 > 0$, in the neighborhood of sliding surface, $s \times \dot{s} < 0$. Thus, the existence of sliding surface is proven. The reachability of the sliding surface is proven by using reduction to absurdity.

(1) When $s < 0$, $u = 1$, assuming that the sliding surface is unreachable, the system will always be in the shoot-through mode, as shown in Fig. 2 (a). The direct duty cycle D is equal to its maximum limit of 0.5. $v_C = V_C = +\infty$ can be obtained according to Formula (6). Thus, when $k_1 > 0, k_3 < 0$, $\dot{s} = k_1 \times \frac{v_C}{L} + k_2 \times \frac{i_L}{L} + k_3 \times (V_C^* - v_C) > 0$.

(2) When $s > 0$, $u = 0$, assuming that the sliding surface is unreachable, the system will always be in the non-shoot-through mode, as shown in Fig. 2 (b). The direct duty cycle D is equal to its minimum limit of 0. $v_C = V_C = V_{in}$ and $i_L = I_L = I_{load} = \frac{V_{dc}^* v_C}{R_L V_C^*}$ can be obtained according to Formulas (6) and (7). Thus, when $k_3 < 0$, $\dot{s} = k_3 \times (V_C^* - V_{in}) < 0$.

Combining (1) and (2), we can obtain the following: assuming that the sliding surface is unreachable, when $k_1, k_2 > 0$ and $k_3 < 0$, $s \times \dot{s} < 0$. Thus, the assumption is invalid, and the reachability of sliding surface is proven. The stability is then deduced. Formula (10) is integrated into Formula (12) and then made it equal to 0. The equivalent control rate can be obtained as

$$u_{eq} = \frac{\begin{matrix} k_1 C(v_C - V_{in}) + k_2 L(i_L - \frac{V_{dc}^* v_C}{R_L V_C^*}) \\ -k_3 L C(V_C^* - v_C) \end{matrix}}{k_1 C(2v_C - V_{in}) + k_2 L(i_L - \frac{V_{dc}^* v_C}{R_L V_C^*})} \tag{17}$$

Formula (17) is substituted into Formula (10), and we can obtain

$$\begin{bmatrix} \dot{x}_1 \\ \dot{x}_2 \\ \dot{x}_3 \end{bmatrix} = \begin{bmatrix} -k_2 \frac{V_{dc}^* v_c^2}{R_L V_C^*} + k_2 V_{in} i_L + k_3 C(2v_c^2 - \\ 2v_C V_C^* - i_L V_{in} + V_C^* V_{in})]/k_1 \\ [k_1(i_L V_{in} - \frac{V_{dc}^* v_c^2}{R_L V_C^*}) + k_3 L(2i_L - \\ \frac{V_{dc}^* v_C}{R_L V_C^*})(v_C - V_C^*)]/[k_1 C(V_{in} - \\ 2v_C) + k_2 L(2i_L - \frac{V_{dc}^* v_C}{R_L V_C^*})] \\ V_C^* - v_C \end{bmatrix} \tag{18}$$

$\dot{x}_3$ is independent of k_1, k_2 in Formula (18); thus, the first two components of Formula (18), $\dot{x}_1$ and $\dot{x}_2$, are analyzed. The right end is set equal to 0, and we can obtain

$$i_L = \frac{V_{dc}^* V_C^* v_C}{R_L V_C^* V_{in}} = \frac{I_{load} V_C^*}{V_{in}}$$
$$v_C = V_C^* \tag{19}$$

The equilibrium point of the equation is

$$\begin{bmatrix} x_1 \\ x_2 \end{bmatrix} = \begin{bmatrix} \frac{I_{load} V_C^*}{V_{in}} \\ 0 \end{bmatrix} \tag{20}$$

When the disturbance is introduced into the neighborhood of the equilibrium point, the linearization of the small-signal state equation can be expressed as

$$\begin{cases} \frac{d\Delta x_1}{dt} \approx \frac{1}{b}(a_{11}\Delta x_1 + a_{12}\Delta x_2) \\ \frac{d\Delta x_2}{dt} \approx \frac{1}{b}(a_{21}\Delta x_1 + a_{22}\Delta x_2) \end{cases} \tag{21}$$

where $b = k_1 C(V_{in} - 2V_C^*) + k_2 L(\frac{2V_C^*}{V_{in}} - 1)I_{load}$; $A = \begin{bmatrix} a_{11} & a_{12} \\ a_{21} & a_{22} \end{bmatrix} = \begin{bmatrix} k_2 V_{in} & -k_2 I_{load} + 2k_3 C V_C^* - k_3 C V_{in} \\ k_1 V_{in} & (\frac{2k_3 L V_C^*}{V_{in}} - k_1 - k_3 L)I_{load} \end{bmatrix}$.

If the eigenvalues of matrix A have a negative real part, then the equilibrium point of Formula (18) is asymptotically stable. The stability of the entire closed-loop system can be
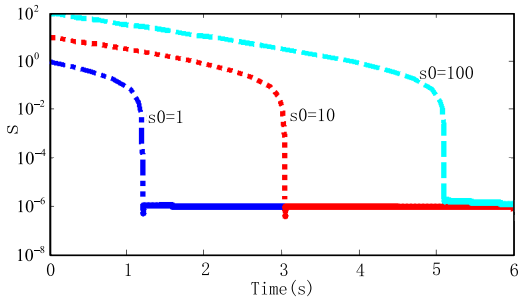
FIGURE 4. Simulation results of the sliding surface *s* under the control of the exponential approaching law.

guaranteed. Thus,

$$
\begin{cases}
k_1^2 + (k_2 V_{in} + \dfrac{2k_3 L V_C^*}{V_{in}})^2 + 2k_1 k_2 (2I_{load} - 1) V_{in} \\
\quad + 4k_1 k_3 [C V_{in}(V_{in} - 2V_C^*) - \dfrac{L V_C^*}{V_{in}}] < 0 \\
(k_1 + k_2 V_{in} - \dfrac{2k_3 L V_C^*}{V_{in}})[k_1 C(V_{in} - 2V_C^*) \\
\quad + k_2 L I_{load}(\dfrac{2V_C^*}{V_{in}} - 1)] < 0
\end{cases}
\tag{22}
$$

If k_1, k_2 and k_3 are determined in accordance with Formula (22), then the entire system is guaranteed to be asymptotically stable. Thus, the stability of the system is proven.

B. APPROACHING LAW DESIGN
The existence and reachability of the sliding surface are satisfied when the movement point at any position in the state space can reach the sliding surface during a limited period. At this time, the specific trajectory of the movement point is unspecified. We propose the "approaching law" to improve the dynamic performance of this movement. Traditional approaching laws include exponential, power, and general approximation laws. The exponential approach law is often used.

$$ \dot{s} = -\varepsilon sgn(s) - \xi_e s \quad \varepsilon > 0, \xi_e > 0 \tag{23} $$

When $s > 0$, $\dot{s} = -\varepsilon - \xi_e s$, the following equation may be solved:

$$ s(t) = -\frac{\varepsilon}{\xi_e} + (s_0 + \frac{\varepsilon}{\xi_e})e^{-\xi_e t} \tag{24} $$

When $s < 0$, $\dot{s} = +\varepsilon - \xi_e s$, the following equation may be solved:

$$ s(t) = \frac{\varepsilon}{\xi_e} + (s_0 - \frac{\varepsilon}{\xi_e})e^{-\xi_e t} \tag{25} $$

where S_0 is the value of the sliding surface function $s(x(t))$ in the initial state ($t = 0$) of the system. The exponential approaching law (EAL) cannot eliminate chattering because it contains constant terms. We use $\varepsilon = 0.4, \xi_e = 1.1$ as an example. We separately consider $s_0 = 1, s_0 = 10$ and $s_0 = 100$. The sliding surface *s* of the system can be obtained under the control of EAL. The simulation results are shown in Fig. 4 (i.e., the vertical axis of the figure contains logarithmic coordinates for a clear presentation).

Under the EAL control, the convergence time of the sliding-mode surface *s* increases significantly, and the convergence speed is slow as the initial value s_0 of the sliding surface function increases (see Fig. 4). In practice, it is difficult to find a suitable initial value for the sliding surface. Accordingly, combining (12) and (23) yields the following equation:

$$ k_1 \times \dot{x}_1 + k_2 \times \dot{x}_2 + k_3 \times \dot{x}_3 = -\varepsilon sgn(s) - \xi_e s \tag{26} $$

From Formula (10), a sliding-mode controller based on EAL can be obtained.

$$ u_c = \frac{\begin{array}{l} k_1 CR_L V_C^*(V_{in} - v_C) + k_2 L(V_{dc}^* v_C - R_L V_C^* i_L) \\ + CLR_L V_C^*[k_3 V_C^* + \varepsilon sgn(s) + \xi_e s - k_3 v_C] \end{array}}{k_2 L(V_{dc}^* v_C - 2R_L V_C^* i_L) + k_1 CR_L V_C^*(V_{in} - 2v_C)} \tag{27} $$

The MPAL used in this study is as follows:

$$ \dot{s} = -\xi_1 |s|^\alpha sgn(s) - \xi_2 |s|^\beta sgn(s) - \xi_3 |s|^\gamma sgn(s) - \xi_4 s \tag{28} $$

where $\xi_1 > 0, \xi_2 > 0, \xi_3 > 0, \xi_4 > 0, \alpha > 1$ and $0 < \beta < 1$. The value of γ is as follows:

$$ \gamma = \begin{cases} \max\{\alpha, |s|\}, & |s| \geq 1 \\ \min\{\beta, |s|\}, & |s| < 1 \end{cases} \tag{29} $$

(1) When $|s| < 1$, the approaching law (28) is mainly affected by $-\xi_2 |s|^\beta sgn(s) - \xi_3 |s|^\gamma sgn(s)$ based on the property of the power function. γ value adaptively changes the exponential parameters based on β and $|s|$ to achieve an optimal approaching process. (2) When $|s| \geq 1$, the approaching law (28) is mainly affected by $-\xi_1 |s|^\beta sgn(s) - \xi_3 |s|^\gamma sgn(s)$. The value of γ adaptively changes the exponential parameters based on α and $|s|$ to achieve an optimal approaching process. From Formula (28), the following formula is obtained:

$$ s\dot{s} = -\xi_1 |s|^{\alpha+1} - \xi_2 |s|^{\beta+1} - \xi_3 |s|^{\gamma+1} - \xi_4 s^2 \leq 0 \tag{30} $$

Thereafter, the designed sliding-mode approximation law becomes existent and reachable, i.e., the system state *s* in the law of convergence (28) can be achieved under the balance point $s = 0$. When $s = 0$, the approaching law (28) can be written as $\dot{s} = 0$, i.e., the system in the vicinity of the steady state does not produce chattering.

We consider $\xi_1 = 1.5, \xi_2 = 0.8, \xi_3 1.2, \xi_4 = 0.9, \alpha = 1.5$ and $\beta = 0.5$ and separately consider $s_0 = 1, s_0 = 10, s_0 = 100$. The sliding surface *s* of the system can be obtained under the MPAL control. The simulation results are shown in Fig. 5.

Under the MPAL control, the convergence time increment of the sliding-mode surface *s* is small, particularly after $s_0 > 1$ (see Fig. 5). Under the influence of this control rate, the convergence time is nearly constant. Regardless of whether the initial state of the system is far from the sliding surface, the control rate can immediately reach the sliding surface and converge rapidly. We consider $s_0 = 100$. The simulation results of the sliding-mode surface *s* of the system
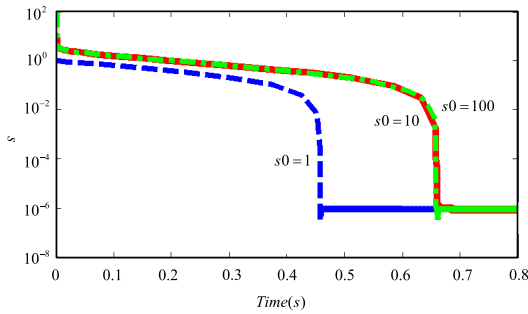
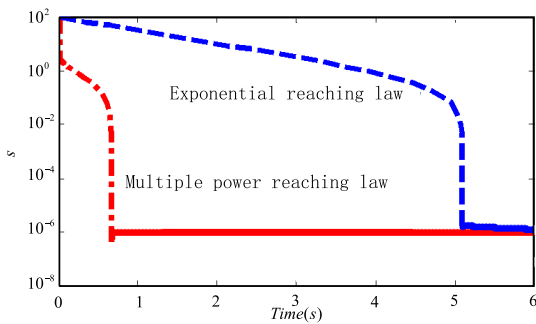**FIGURE 5.** Simulation results of the sliding surface *s* under the control of MPAL.

FIGURE 6. Comparison of the simulation results of the sliding surface *s* controlled by MPAL and exponential approaching law.

(a) input voltage changes with EAL

(b) input voltage changes with MPAL

FIGURE 7. Simulation results of the DC-link voltage and capacitance voltage under EAL and MPAL when input voltage changes.

can be obtained and controlled with MPAL and EAL, respectively. The simulation results are shown in Fig. 6.

When s_0 is 100, the sliding surface is reached in 5.1 and 0.65 s under EAL and MPAL, respectively (see Fig. 6). The control speed of MPAL is 10 times faster than that of EAL, particularly in the initial stage. If the value of γ is extremely large under MPAL in the initial stage, then the value of s can be immediately decreased to approximately 10. However, the same cannot be realized under EAL. Combining Formulas (12) and (28) yields the following formula:

$$k_1 \times \dot{x}_1 + k_2 \times \dot{x}_2 + k_3 \times \dot{x}_3 = -\xi_1 |s|^{\alpha} sgn(s)$$
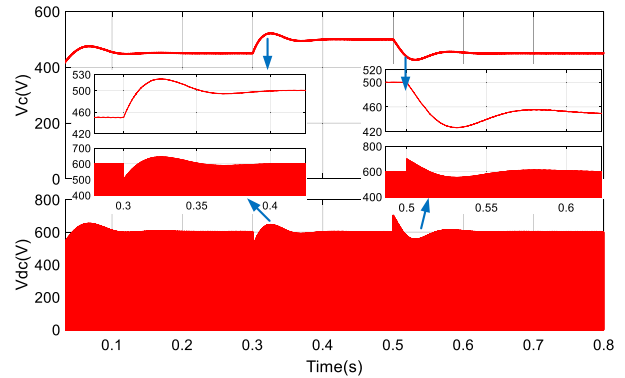$$-\xi_2 |s|^{\beta} sgn(s) - \xi_3 |s|^{\gamma} sgn(s) - \xi_4 s \quad (31)$$

From Formula (10), a sliding-mode controller based on MPAL can be obtained.

$$u_c = \frac{k_1 C R_L V_C^* (V_{in} - v_C) + k_2 L (V_{dc}^* v_C - R_L V_C^* i_L) + C L R_L V_C^* [k_3 V_C^* - \dot{s} - k_3 v_C]}{k_2 L (V_{dc}^* v_C - 2R_L V_C^* i_L) + k_1 C R_L V_C^* (V_{in} - 2v_C)}$$
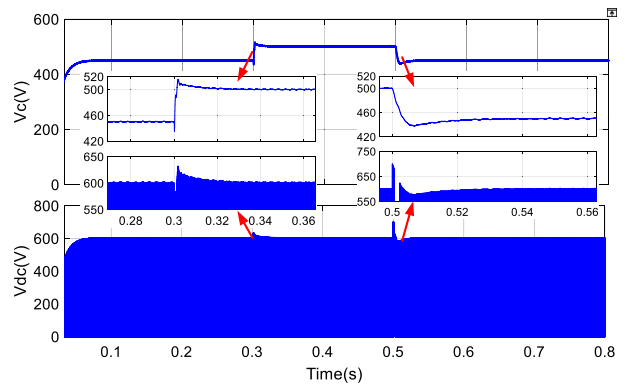$$(32)$$

The above formula is the direct duty cycle D in the control system mentioned previously.

V. SIMULATION AND EXPERIMENT
The performance of the sliding-mode controller with MPAL is verified in this study. A simulation model of a Z-source inverter based on two control methods is established. The control methods are the traditional EAL and MPAL.

The model is simplified by replacing the solar array with a DC voltage source. The Z-source network parameters are set as follows: the initial input voltage is $300V$, the reference value of the DC-link voltage is $600V$, the switching frequency f_s is $10kHz$, $L = 800\mu F$, and $C = 400\mu F$.

A. SIMULATION RESULTS
When the input voltage increases from $300V$ to $400V$ at $0.3s$, and reduces from $400V$ to $300V$ at $0.5s$, respectively, the output waveform simulation results under the traditional EAL and MPAL-based Z-source network are shown in Fig. 7(a)and Fig. 7(b), respectively. The parameters represent the DC-link voltage and capacitor voltage. Under the sliding-mode control of MPAL (see Fig. 7(b)), the DC-link voltage substantially retains the reference value when the input voltage changes. In the event of sudden disturbance, the system overshoot is 3.2% and the settling time is $20ms$, which are similar to the case of the capacitor voltage. However, Fig. 7(a) shows that under the sliding-mode control of EAL, the DC-link voltage overshoot is 6%, and the settling time is $100ms$ as the input voltage changes, which is significantly greater than the time of the system under the sliding-mode control of MPAL. Comparison of capacitance voltage waveform shows that the capacitor voltage overshoot under the sliding-mode control of MPAL is smaller than that of the system under the sliding-mode control of EAL, and the settling time is relatively small.
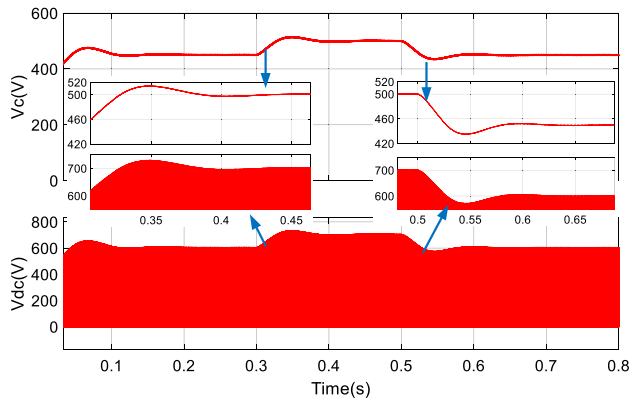
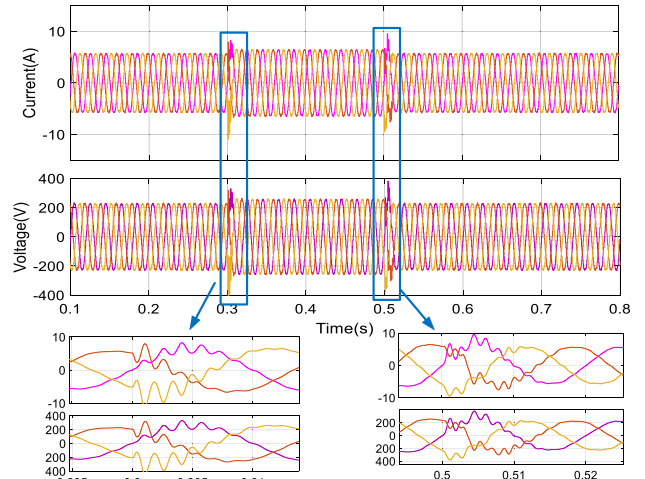(a) the reference value of the DC-link voltage changes with EAL
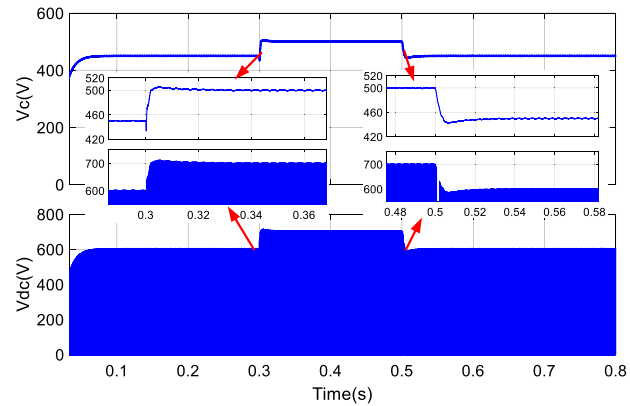
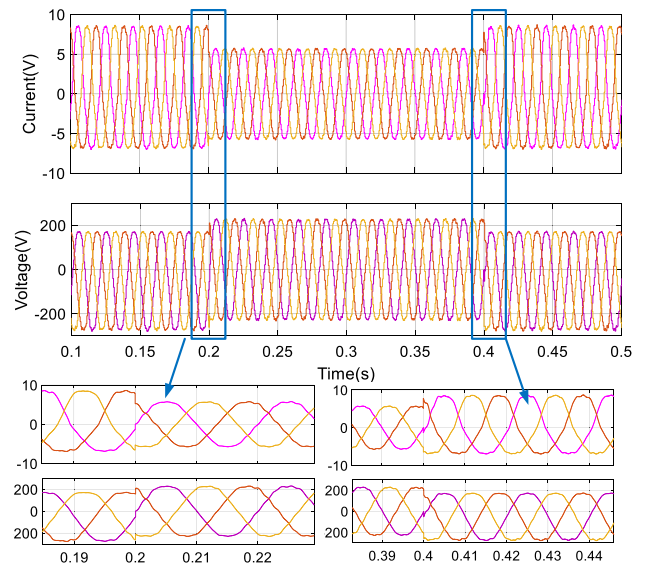(b) the reference value of the DC-link voltage changes with MPAL

FIGURE 8. Simulation results of DC-link voltage and capacitance voltage under EAL and MPAL when the reference value of the DC-link voltage changes.

FIGURE 9. Load voltage and current waveforms under MPAL when input voltage changes.

FIGURE 10. Inverter output voltage and current waveforms under MPAL when load changes.

If the reference value of the DC-link voltage changes from $600V$ to $700V$ at $0.3s$, and reduces from $700V$ to $600V$ at $0.5s$, respectively. The simulation results of the sliding-mode control under EAL and MPAL are shown in Fig. 8(a) and Fig. 8(b), respectively. When the reference voltage changes, the DC-link voltage and capacitor voltage rapidly change into the next stable state under the sliding-mode control with MPAL. The system overshoot is 1%, and the settling time is $10ms$. By contrast, the system overshoot is 4% and the settling time is $90ms$ under the sliding-mode control with EAL. The results indicate that the sliding-mode control with MPAL features anti-interference and a rapid response.

The output voltage and current of the inverter when input voltage changes under the sliding-mode control with MPAL are shown in Fig. 9. The inverter output voltage and current when load changes under the sliding-mode control with MPAL are shown in Fig. 10. Regardless of how input voltage or load changes, the inverter output voltage and current can immediately reach a stable state within 10 ms under the sliding-mode controller with MPAL (see Figs. 10 and 11). The rapid response of the sliding-mode control with MPAL is verified.

B. EXPERIMENTAL RESULTS

The effect of the proposed control strategy is further verified. An RT-LAB real-time simulator is used as a controller. The results are as follows. The experimental parameters are selected based on the aforementioned simulation. The hardware in the loop simulation experiment platform is shown in Fig. 11.

RT-LAB is a set of industrial system real-time simulation platform launched by Opal-RT Technologies Corporation of Canada. By applying this open and extensible real-time platform, we can apply the dynamic system mathematical model established by MATLAB to real-time simulation, control, test, and other related fields directly. The experimental research of Z-source PV
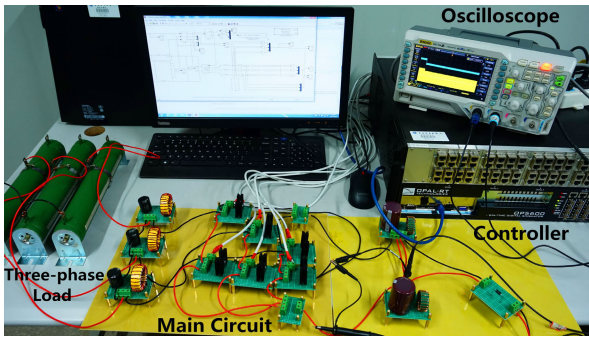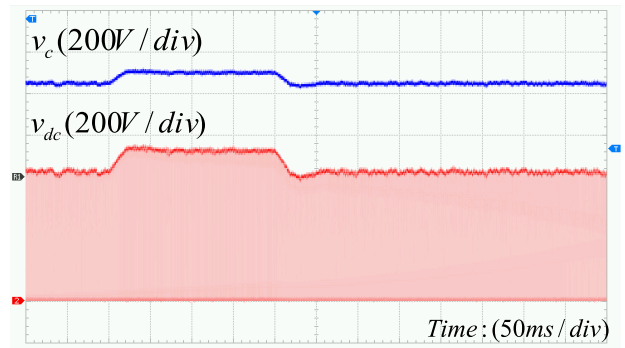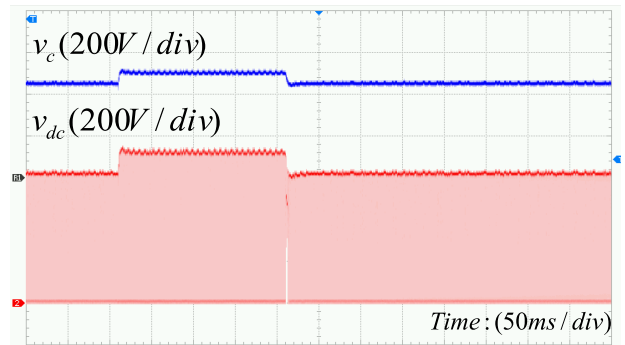
FIGURE 11. Hardware in the loop simulation experiment platform.

(a) input voltage changes with EAL

(b) input voltage changes with MPAL

FIGURE 12. Simulation results of the DC-link voltage and capacitance voltage under EAL and MPAL when input voltage changes.

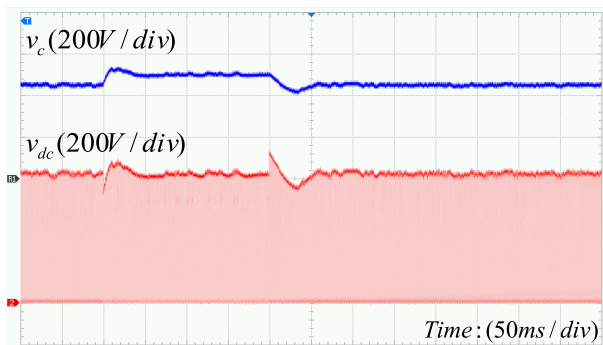(a) the reference value of the DC-link voltage changes with EAL

(b) the reference value of the DC-link voltage changes with MPAL
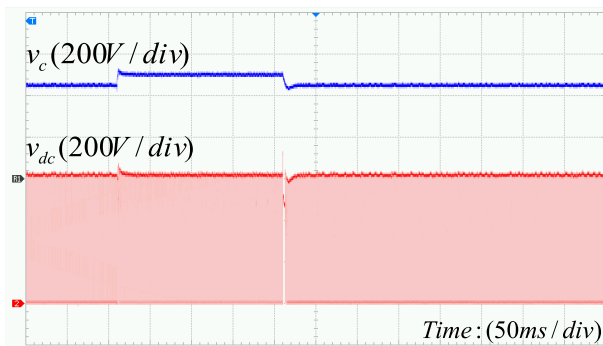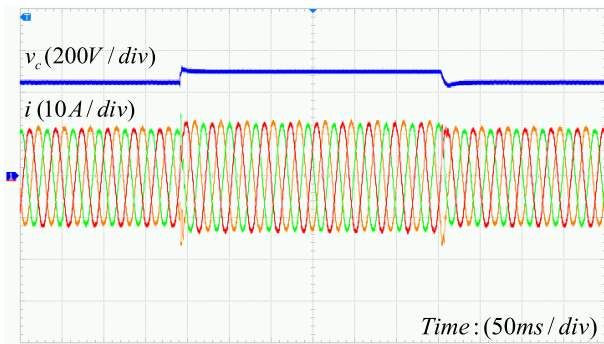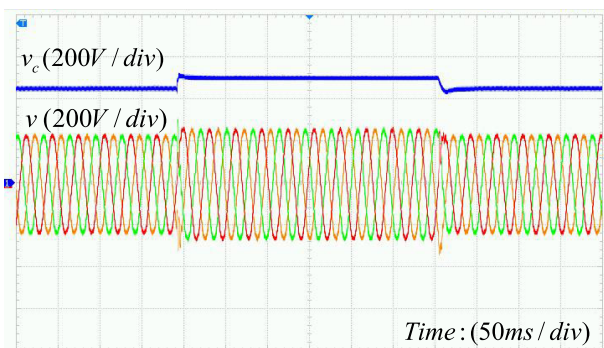
FIGURE 13. Simulation results of DC-link voltage and capacitance voltage under EAL and MPAL when the reference value of the DC-link voltage changes.

inverter is conducted on the hardware in the loop simulation experiment platform based on RT-LAB to verify the good performance of the control strategy designed in this study. The experimental hardware includes DC power supply, main circuit of Z-source inverter, RT-LAB simulator, and load. The software includes MATLAB/Simulink, RT-LAB main program, and RT-Events toolbox. The Z-source network parameters are set as follows: the initial input voltage is $300V$, the reference value of the DC-link voltage is $600V$, the switching frequency f_s is $10kHz$, $L = 800\mu H$, and $C = 400\mu F$. The output voltage amplitude is $220V$, and the frequency is $50Hz$. The load resistor $R_L = 20\Omega$, and the load power is $1.1kw$.

When the input voltage changes from $300V$ to $400V$, and reduces from $400V$ to $300V$, the output waveform experimental results under the traditional EAL and MPAL-based Z-source network are shown in Fig. 12. Under the sliding-mode control of MPAL (see Fig. 12(b)), when the input voltage increases suddenly or sags, the DC-link voltage is only slightly jitter at the mutation, returns to its original value in a very short time, and remains unchanged. In the event of sudden disturbance, the system overshoot is less than 4% and the settling time is $10ms$, which are similar to the case of the capacitor voltage. This result is consistent with the simulation results, which verifies the correctness of the experimental results. However, Fig. 12(a) shows that under the sliding-mode control of EAL, when the input voltage increases suddenly or sags, the DC-link voltage exhibits a larger overshoot at the abrupt change, and the dynamic response is slower. The DC-link voltage overshoot is greater than 10% and the settling time is greater than $50ms$ as the input voltage changes, which is significantly greater than the time of the system under the sliding-mode control of MPAL.

By comparing the two control methods, we can conclude that the MPAL-based sliding-mode control shows an improved performance in anti-disturbance and dynamic response compared with that based on EAL. When the reference value of V_{dc} gradually increases from $600V$ to $700V$ thereafter and gradually reduces from $700V$ to $600V$,

(a) Load current waveform when input voltage changes

(b) Load voltage waveform when input voltage changes

FIGURE 14. **Load voltage and current waveforms when input voltage changes.**

the output waveform experimental results of the DC-link voltage under the two controllers are shown in Fig. 13. Under the sliding-mode control of MPAL (see Fig. 13(b)), regardless of the reference voltage increase or decrease, the DC-link voltage and capacitor voltage will soon move to the next stable state. The DC-link voltage overshoot is 1.2%, and the settling time is less than 10ms. By contrast, Fig. 13(a) shows that under the sliding mode-control of EAL, the overshoot of the system is 4.67%, and the settling time is greater than 30ms. This result is basically consistent with the simulation results. By comparing the two figures, we can conclude that under the sliding-mode control of MPAL, when the reference value changes, the DC-link voltage and capacitor voltage are able to respond rapidly. The MPAL-based sliding-mode control has a fast dynamic response and robustness compared with that based on EAL.

The output voltage and current waveforms of the inverter when the input voltage changes under the sliding-mode control with MPAL are shown in Fig. 14. The system immediately reaches a stable state, thereby providing good anti-disturbance and a dynamic response.

VI. CONCLUSION

The non-minimum phase is an issue in controlling Z-source PV inverter systems. This study analyzes the working principle of a Z-source PV inverter and considers capacitor voltage difference and inductor current as variables to establish a

sliding surface based on sliding-mode control theory. MPAL is adopted to ensure the good performance of the Z-source DC-link voltage control. Simulation and experimental results verify the effect of sliding-mode control with MPAL relative to the sliding-mode control with EAL. The results show that the system overshoot is greater than 4% and the settling time is greater than 30ms under the sliding-mode control of EAL. Under the sliding-mode control of MPAL, the system overshoot is close to 1.2%, and the settling time is less than 10ms. The sliding-mode control with MPAL features a rapid response, high stability, and strong robustness compared with that based on EAL.

REFERENCES

[1] F. Z. Peng, "Z-source inverter," *IEEE Trans. Ind. Appl.*, vol. 39, no. 2, pp. 504–510, Mar./Apr. 2003.

[2] J. J. Soon and K.-S. Low, "Sigma-Z-source inverters," *IET Power Electron.*, vol. 8, no. 5, pp. 715–723, May 2015.

[3] H. Fathi and H. Madadi, "Enhanced-boost Z-source inverters with switched Z-impedance," *IEEE Trans. Ind. Electron.*, vol. 63, no. 2, pp. 691–703, Feb. 2016.

[4] S. Divya and V. Prabhu, "High voltage improved trans-Z-source inverter," in *Proc. IEEE Int. Conf. Elect. Energy Syst.*, vol. 21, Oct. 2014, pp. 255–260.

[5] M.-K. Nguyen, Y.-C. Lim, S.-J. Park, and D.-S. Shin, "Family of high-boost Z-source inverters with combined switched-inductor and transformer cells," *IET Power Electron.*, vol. 6, no. 6, pp. 1175–1187, Jul. 2013.

[6] M.-K. Nguyen, Y.-C. Lim, and Y.-J. Kim, "A modified single-phase quasi-Z-source AC–AC converter," *IEEE Trans. Power Electron.*, vol. 27, no. 1, pp. 201–210, Jan. 2012.

[7] J. R. Rahul and A. Kirubakaran, "Single-phase quasi-Z-source based isolated DC/AC converter," in *Proc. IEEE Int. Conf. Power Syst.*, Mar. 2016, pp. 1–4.

[8] S. Jiang, D. Cao, and F. Z. Peng, "High frequency transformer isolated Z-source inverters," in *Proc. IEEE Appl. Power Electron. Conf. Expo.*, Mar. 2011, pp. 442–449.

[9] O. Ellabban, J. Van Mierlo, and P. Lataire, "A DSP-based dual-loop peak DC-link voltage control strategy of the Z-source inverter," *IEEE Trans. Power Electron.*, vol. 27, no. 9, pp. 4088–4097, Sep. 2012.

[10] Y. Zhang, J. Shi, L. Zhou, J. Li, M. Sumner, P. Wang, and C. Xia, "Wide input-voltage range boost three-level DC–DC converter with quasi-Z source for fuel cell vehicles," *IEEE Trans. Power Electron.*, vol. 32, no. 9, pp. 6728–6738, Sep. 2017.

[11] A. Ayad, P. Karamanakos, and R. Kennel, "Direct model predictive current control strategy of quasi-Z-source inverters," *IEEE Trans. Power Electron.*, vol. 32, no. 7, pp. 5786–5801, Jul. 2017.

[12] N. Sabeur, S. Mekhilef, and A. Masaoud, "Extended maximum boost control scheme based on single-phase modulator for three-phase Z-source inverter," *IET Power Electron.*, vol. 9, no. 4, pp. 669–679, Mar. 2016.

[13] Q. Sun and Y. Wang, "Integral sliding mode control of Z-source inverter for motor drive system of electric vehicles," in *Proc. World Congr. Intell. Control Autom.*, vol. 26, Jul. 2012, pp. 6–8.

[14] J. Liu, S. Jiang, D. Cao, and F. Z. Peng, "A digital current control of quasi-Z-source inverter with battery," *IEEE Trans. Ind. Informat.*, vol. 9, no. 2, pp. 928–937, May 2013.

[15] U. K. Shinde, S. G. Kadwane, S. P. Gawande, M. J. B. Reddy, and D. K. Mohanta, "Sliding mode control of single-phase grid-connected quasi-Z-source inverter," *IEEE ACCESS*, vol. 5, pp. 10232–10240, 2017.

[16] R. Ling, D. Maksimovic, and R. Leyva, "Second-order sliding-mode controlled synchronous buck DC–DC converter," *IEEE Trans. Power Electron.*, vol. 31, no. 3, pp. 2539–2549, Mar. 2016.

[17] A. Abrishamifar, A. A. Ahmad, and M. Mohamadian, "Fixed switching frequency sliding mode control for single-phase unipolar inverters," *IEEE Trans. Power Electron.*, vol. 27, no. 5, pp. 2507–2514, May 2012.

[18] R. Xu and M. Zhou, "Sliding mode control with sigmoid function for the motion tracking control of the piezo-actuated stages," *Electron. Lett.*, vol. 53, no. 2, pp. 75–77, Jan. 2017.

[19] C. Zhang, Z. Lin, S. X. Yang, and J. He, ''Total-Amount Synchronous Control Based on Terminal Sliding-Mode Control,'' *IEEE Access*, vol. 5, pp. 5436–5444, 2017.

[20] S. M. Mozayan, M. Saad, H. Vahedi, H. Fortin-Blanchette, and M. Soltani, ''Sliding mode control of PMSG wind turbine based on enhanced exponential reaching law,'' *IEEE Trans. Ind. Electron.*, vol. 63, no. 10, pp. 6148–6159, Oct. 2016.

[21] A. Wang, X. Jia, and S. Dong, ''A new exponential reaching law of sliding mode control to improve performance of permanent magnet synchronous motor,'' *IEEE Trans. Magn.*, vol. 49, no. 5, pp. 2409–2412, May 2013.

[22] K. Liu, Y. Cao, S. Wang, and Y. Li, ''Terminal sliding mode control for landing on asteroids based on double power reaching law,'' in *Proc. IEEE Int. Conf. Inf. Autom.*, Aug. 2015, pp. 2444–2449.

[23] H. Zaman, X. Zheng, S. Khan, H. Ali, and X. Wu, ''Hysteresis modulation-based sliding mode current control of Z-source DC-DC converter,'' in *Proc. IEEE Power Electron. Motion Control Conf.*, May 2016, pp. 22–26.

[24] Y. Guo, Y. Zhang, G. Ma, and T. Zeng, ''Multi-power sliding mode guidance for Mars powered descent phase,'' in *Proc. IEEE Int. Conf. Control*, Aug./Sep. 2016, pp. 1–6.

[25] J. Song, Y. Niu, and Y. Y. Zou, ''Finite-time stabilization via sliding mode control,'' *IEEE Trans. Autom. Control*, vol. 62, no. 3, pp. 1478–1483, Mar. 2017.

YAN CHEN received the M.S. degree in measuring and testing technologies and instruments from the Chongqing University of Technology, in 2008, and the Ph.D. degree in electrical engineering from Chongqing University, in 2012. From March 2015 to September 2015, she was a Visiting Scholar with the Korea Advanced Institute of Science and Technology. She is currently an Associate Professor with the School of Electrical and Electronic Engineering, Chongqing University of Technology. She has published more than 30 journal and conference articles, such as the IEEE Transactions on Power Electronics and *Journal of Control Theory and Applications*. Her research interests include power electronic devices and systems, and nonlinear control technology.

RUI TAN was born in Chongqing, China, in 1995. She received the B.S. degree in electrical engineering and automation from Shanghai Normal University, Shanghai, China, in 2018. She is currently pursuing the M.S. degree with the Chongqing University of Technology, Chongqing. Her current research interests include new energy generation and control technology.

YONG ZHENG received the B.S. degree in mechanical engineering and automation from the Qingdao University of Science and Technology, Qingdao, China, in 2005, the M.S. degree in measuring and testing technologies and instruments from the Chongqing University of Technology, in 2008, and the Ph.D. degree in measuring and testing technologies and instruments from the Hefei University of Technology, in 2012. He is currently an Assistant Professor with the Engineering Research Center of Mechanical Testing Technology and Equipment, Ministry of Education, Chongqing University of Technology, and he is particularly interested in electrical detection and control.

ZHIYANG ZHOU was born in Jiulongpo, Chongqing, China, in 1996. He received the B.S. degree in electrical engineering from the City College of Science and Technology, Chongqing University, in 2018. He is currently pursuing the M.S. degree in electrical engineering with the Chongqing University of Technology. His current research interest includes nonlinear dynamic behavior of power electronics.

● ● ●